On the long-range correlations in hadron-nucleus collisions

N.Armesto[a], M.A.Braun[b] and C.Pajares[a]

[a] Departamento de Física de Partículas and IGFAE,
Universidade de Santiago de Compostela, 15782 Santiago de Compostela, Spain

[b] Department of High-Energy Physics, St. Petersburg University,
198504 St. Petersburg, Russia

Abstract

Long-range correlations between multiplicities in different rapidity windows in hadron-nucleus collisions are analyzed. After recalling the standard results in the probabilistic model, we study them in the framework of perturbative QCD. Considering interacting BFKL pomerons in the form of fan diagrams coupled to a dilute projectile, analytic estimates are done for very large rapidities. The correlation strength results weakly depending on energy and centrality or nuclear size, and generically greater than unity. Finally, we turn to the Color Glass Condensate framework. For a saturated projectile, the resulting correlation strength turns out to be smaller than unity and decreasing with increasing energy. Its behavior with increasing centrality or nuclear size depends on the considered rapidity windows.

1 Introduction

Long-range correlations have been attracting much attention since long ago in the region of both low and high transverse momenta of secondaries. At low momenta the color string picture [1] with fusion and percolation effects [2] has been extensively applied [3, 4]. In the semihard region the Color Glass Condensate (CGC) picture has lately been used [5, 6]. One can separate long-range correlations into a contribution from purely hadronic collisions and another coming from the effects generated by the heavy nucleus target or/and projectile. Obviously the first contribution can hardly be treated in a more or less rigorous theoretical framework due to the essentially non-perturbative structure of the hadron. Heavy nucleus collisions, on the other hand, present more opportunities in this sense, due to their comparatively simple structure in terms of constituent nucleons. Single inclusive cross-sections with participation of nuclei can be easily found even in the framework of interacting pomerons, both of the old local type and of the sophisticated Balitsky-Fadin-Kuraev-Lipatov (BFKL)

type. In the limit of very heavy nuclei they are expressed in terms of the sum of the corresponding pomeron fan diagrams. However long-range correlations require also knowledge of the double inclusive cross-section, for which the situation is more complicated. In the purely eikonal approach they can also be easily calculated from the known single and double elementary (hadron-nucleon) inclusive cross-sections. However with interacting pomerons this is only possible for the hadron-nucleus case. Double inclusive cross-section for nucleus-nucleus scattering mediated by interacting pomerons involves a complicated set of diagrams, exact summation of which does not look feasible. So hadron-nucleus collisions present a subject better suited for theoretical discussion of long-range correlations in the nuclear background.

In this paper we study long-range correlations in hadron-nucleus collisions in the hard domain. We shall use two different approaches to this problem, which treat different range of energies. At very high (asymptotic) energies we shall rely on the perturbative Quantum Chromodynamics (QCD), which predicts that the interaction is mediated by interacting BFKL pomerons while treating the hadron as a dilute object through the whole evolution. At smaller energies, when evolution of the gluon density is not complete, we shall apply the Color Glass Condensate approach, in which the fast nucleus is represented by a strong classical gluon field [7]. This approach has been lately used for a qualitative study of correlations in nucleus-nucleus collisions with promising results [6].

The paper is organized as follows. In the next section, to have a basis for comparison and discussion, we shall recall some basic predictions for the long-range correlations in hA collisions, which follow from the straightforward probabilistic approach. Section 3 is dedicated to the perturbative QCD approach at very high energies. Section 4 presents some qualitative predictions from the Color Glass Condensate. Finally we discuss our results in the Conclusions.

2 Probabilistic treatment

In this section we shall study long-range correlations in hA collisions, as they follow from purely probabilistic considerations. This approach is realized in the Glauber-eikonal description of hA interactions and also reproduced in Regge approach with non-interacting pomerons. Our basic instrument will be the standard Glauber expression for the cross-section σ_n for n inelastic interactions of the projectile inside the nucleus:

$$\sigma_n = C_A^n \Big(\sigma T(b)\Big)^n \Big(1 - \sigma T(b)\Big)^{A-n}. \tag{1}$$

Here σ is the elementary (hadron-nucleon) cross-section, and $T(b)$ is the standard nuclear profile function normalized to unity. From this expression we immediately derive expressions

for the single and double inclusive cross-sections for hA collisions, J_1 and J_2 respectively. At fixed impact parameter b

$$J_1(y,k) = Aj_1(y,k)T(b) \tag{2}$$

and

$$J_2(y_1,k_1;y_2,k_2) = Aj_2(y_1,k_1;y_2,k_2)T(b) + A(A-1)j_1(y_1,k_1)j_1(y_2,k_2)T^2(b). \tag{3}$$

Here and in the following we denote by small letters the quantities which refer to the elementary hN collision. So j_1 and j_2 are the single and double inclusive cross-sections for hadron-nucleon collisions; y and k denote the rapidity and transverse momentum of the produced particle.

To pass to the corresponding multiplicities we have to integrate over b and divide by the total inelastic hA cross-section Σ^{in}. To do this we have to choose a form of the profile function $T(b)$. We use the simplest choice of the constant nuclear density within a sphere of radius $R_A = A^{1/3}R_0$, which gives

$$T(b) = \frac{2\sqrt{R_A^2 - b^2}}{V_A}, \tag{4}$$

where V_A is the nuclear volume. With this profile function we find

$$\int d^2b T^2(b) = \frac{9}{8}\frac{1}{\pi R_A^2}. \tag{5}$$

For large A, with a good precision, the inelastic hA cross-section $\Sigma^{in} = \pi R_A^2$, so that we finally find the single and double hA multiplicities, M_1 and M_2, respectively as

$$M_1(y,k) = A^{1/3}m_1(y,k) \tag{6}$$

and

$$M_2(y_1,k_1;y_2,k_2) = A^{1/3}m_2(y_1,k_1;y_2,k_2) + \frac{9}{8}A^{2/3}\mu_1(y_1,k_1)m_1(y_2,k_2). \tag{7}$$

With these expressions we can pass to correlations. The strength of long-range correlations in nuclear collisions is standardly determined by the coefficient

$$B = \frac{\langle N_F N_B\rangle - \langle N_F\rangle\langle N_B\rangle}{\langle N_F^2\rangle - \langle N_F\rangle^2}, \tag{8}$$

where N_F and N_B are the numbers of particles produced in two rapidity windows. separated by a sufficiently large rapidity interval ('forward' and 'backward'). Note that in the asymmetric hadron-nucleus case, there is another correlation strength defined with $\langle N_F^2\rangle - \langle N_F\rangle^2$ in the denominator. As to the particle transverse momenta, they may be both taken integrated over the whole phase space or restricted to specific parts of it (even practically fixed). This

circumstance plays no role for the following derivation. The average numbers which figure in (8) are expressed via the multiplicities as follows

$$\langle N_{F(B)}\rangle = \int d\tau^{F(B)} M_1(y,k), \tag{9}$$

$$\langle N_F N_{F(B)}\rangle = \int d\tau_1^F d\tau_2^{F(B)} M_2(y_1,k_1;y_2,k_2), \tag{10}$$

where $d\tau^F$ and $d\tau^b$ denote integration over y and k in the forward and backward windows.

Similar quantities for the elementary hN collisions will be denoted by small letters. So for hN collisions the correlation coefficient is determined as

$$b = \frac{\langle n_F n_B\rangle - \langle n_F\rangle\langle n_B\rangle}{\langle n_F^2\rangle - \langle n_F\rangle^2}\,, \tag{11}$$

where the averages are defined as in (9) and (10) with multiplicities μ_1 and μ_2. Using relations (6) and (7) we can express averages for the nucleus target via the same quantities on the nucleon target to obtain:

$$B = \frac{\langle n_F n_B\rangle + \frac{1}{8}A^{1/3}\langle n_F\rangle\langle n_B\rangle}{\langle n_F^2\rangle + \frac{1}{8}A^{1/3}\langle n_F\rangle^2}. \tag{12}$$

If we define the dispersion squared in the forward window for the elementary collisions as

$$d^2 = \langle n_F^2\rangle - \langle n_F\rangle^2, \tag{13}$$

then we find

$$B = \frac{bd^2 + \left(\frac{1}{8}A^{1/3}+1\right)\langle n_F\rangle\langle n_B\rangle}{d^2 + \left(\frac{1}{8}A^{1/3}+1\right)\langle n_F\rangle^2}. \tag{14}$$

For symmetric windows (relative to hN collisions) we have $\langle n_F\rangle = \langle n_B\rangle$ so that (14) simplifies to

$$B = \frac{bd^2 + \left(\frac{1}{8}A^{1/3}+1\right)\langle n_F\rangle^2}{d^2 + \left(\frac{1}{8}A^{1/3}+1\right)\langle n_F\rangle^2}. \tag{15}$$

If the dispersion squared is much smaller than the particle number squared, which is expected for large enough energies and windows, we find an approximate expression

$$B \simeq 1 - \frac{d^2}{\langle n_F\rangle^2}(1-b)\frac{1}{1+\frac{1}{8}A^{1/3}}\,. \tag{16}$$

As a result we find that in the theoretical limit $A \to \infty$ the nuclear coefficient B tends to unity, the value of the elementary coefficient b having no importance. So, in this limit, long-range correlations are exclusively a consequence of the nuclear environment. Of course for realistic nuclei the term $(1/8)A^{1/3}$ is not large but smaller than unity so that the coefficient B results noticeably smaller than unity. However we also see that its value only weakly depends on A and is mainly determined by the relative dispersion $d/\langle n_F\rangle$ in elementary collisions. All

these effects are due to the presence of the second term in the nuclear multiplicity M_2, Eq. (7). Note that the limiting case $A = 1$ is achieved through the substitution $A^{1/3}/8 \to -1$ in (14), so that the second terms in both the numerator and denominator of this equation vanish and B passes into b.

3 Long-range correlations in high-energy hA collisions in the perturbative QCD

3.1 Formalism

In the perturbative QCD at high energies the interaction between the incoming hadron and the nuclear target is realized by an exchange of BFKL pomerons, which interact between themselves via the triple pomeron vertex. For a heavy nucleus target with $A \gg 1$ and a point-like projectile this interaction is described by a set of pomeron fan diagrams, which are summed by the non-linear Balitsky-Kovchegov equation [8, 9, 10]. If we denote this sum for a fixed impact parameter b, zero total gluon momentum and intergluon transverse distance r as $\Phi(y, r, b)$ then function $\phi(y, r, b) = \Phi(y, r, b)/(2\pi r^2)$, transformed into momentum space, satisfies the equation

$$\frac{\partial\phi(y, q, b)}{\partial\bar{y}} = -H\phi(y, q, b) - \phi^2(y, q, b), \tag{17}$$

where H is the BFKL Hamiltonian (see e.g [11]) and $\bar{y} = \bar{\alpha}y$ is a rescaled rapidity with the standard notation $\bar{\alpha} = \alpha_s N_c/\pi$. The physical meaning of ϕ is provided by its relation to the gluon density in the nucleus:

$$\frac{d\Big(xG(x, k^2, b)\Big)}{d^2k d^2b} = \frac{N_c^2}{2\pi^3}\frac{1}{\bar{\alpha}}h(y, k, b), \tag{18}$$

where

$$h(y, k, b) = k^2\nabla_k^2\phi(y, k, b) \tag{19}$$

and $y = \ln(x_0/x)$ with x_0 some initial value of x, usually taken ~ 0.01. Function h satisfies a normalization condition

$$\int \frac{d^2k}{2\pi k^2}h(y, k, b) = 1. \tag{20}$$

Numerical calculations [12] show that starting from $\bar{y} \simeq 2$ it develops a scaling structure

$$h(y, k, b) = h(\xi) = 0.295\ \exp(-\xi^2/3.476), \quad \xi = \ln\Big(k/Q_s(y, b)\Big), \tag{21}$$

where $Q_s(y, b)$ is the so-called saturation momentum, which grows exponentially with y:

$$Q_s(y, b) \simeq a\Big(AT(b)R_0^2\Big)^{2/3}\frac{e^{\Delta_1 y}}{\sqrt{y}}\,. \tag{22}$$

$\Delta_1 = (2.0 \div 2.3)\bar{\alpha}$ and a is a numerical constant[1].

An immediate physical application of this framework is to deep inelastic scattering (DIS), with a highly virtual photon as a projectile. A hadronic analogue of this may be the 'onium', that is a quark-antiquark system of a very short dimension. Realistic hadronic projectiles are not point-like and do not allow for the perturbative treatment. So application of the fan diagram approach to their interaction is strictly speaking not very well justified. For this reason in the following we have to keep in mind an approximate character of our derivation, which assumes that, as in DIS, the projectile hadron interacts with the pomeron only once.

Under this approximation the total hadron-nucleus cross-section is given by

$$\Sigma(Y) = 2 \int d^2b d^2\rho(r) \Phi(Y, r, b), \tag{23}$$

where $\rho(r)$ is the color density of the projectile and Y is the overall rapidity. It may be illustrated graphically as shown in Fig. 1, where the circle with the attached line correspond to function Φ. For a normalizable density $\rho(r)$ and finite nucleus (with the profile function (4)) cross-section $\Sigma = \Sigma^{in}$ turns out to be purely geometric: $\Sigma = 2\pi R_A^2$.

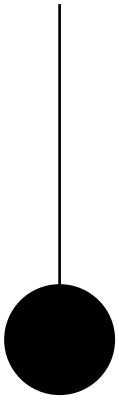

Figure 1: Diagram contributing to the total hA cross-section.

3.2 Single inclusive cross-sections

The single inclusive cross-section is given by the two diagrams shown in Fig. 2 *a* and *b*. They correspond to production of the observed particle either from the pomeron which couples to the projectile or from the vertex of its splitting into a pair of pomerons [14, 15]. All other possibilities are canceled by the Abramovsky-Gribov-Kancheli cutting rules [16]. The sum of

[1]This dependence on impact parameter and nuclear size was obtained [12] for a realistic profile function. Also the value of Δ_1 depends on the rapidity window of the fit, and is slightly small than the asymptotic theoretical expectation, $\Delta_1 = 2.44\bar{\alpha}$. See detailed discussions of these aspects in e.g. [13] where a dependence $\propto A^{1/3}$ is obtained for a cylindrical nucleus. None of these considerations alter the conclusions obtained in this Section.

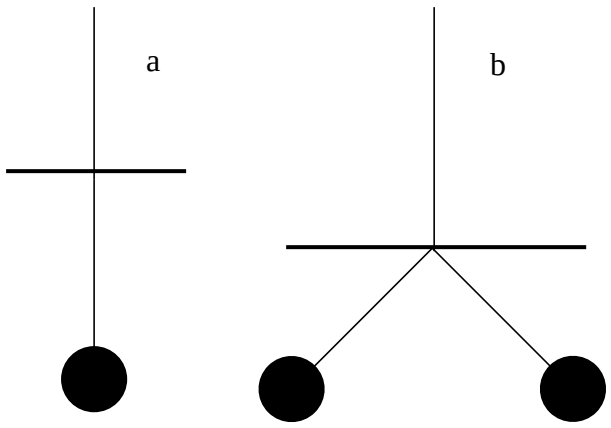

Figure 2: Diagrams contributing to the single inclusive hA cross-section.

these two contributions leads to the single inclusive cross-section at fixed b [17]

$$J_1(y,k,b) = \frac{4\pi\bar{\alpha}}{k^2}\int d^2r e^{ikr}\nabla^2 P(Y-y,r)\nabla^2\Big(2\Phi(y,r,b) - \Phi^2(y,r,b)\Big), \tag{24}$$

where $P(Y-y,r)$ is the pomeron coupled to the projectile:

$$P(Y-y,r) = \int d^2r'\rho(r')G(Y-y,r',r), \tag{25}$$

with the nucleus at $y=0$ and the dilute projectile at $y=Y$, and G is the BFKL forward Green function [11]. Performing the differentiations and passing to momentum space one obtains

$$J_1(y,k,b) = \frac{4\pi\bar{\alpha}}{k^2}\int d^2q h^{(0)}(Y-y,q)w(y,k-q,b). \tag{26}$$

Here $h^{(0)}(y,q)$ is a function analogous to $h(y,q,r)$ for the pomeron, that is a Fourier transform of $\nabla^2 P(y,r)/(2\pi)$. Function $w(y,q,b)$ is defined via $h(y,q,b)$:

$$w(y,q,b) = \frac{q^2}{2\pi}\int d^2q_1 \frac{h(y,q_1,b)h(y,q-q_1,b)}{q_1^2(q-q_1)^2}. \tag{27}$$

It satisfies the same normalization condition (20) and has the same scaling property (21), although with a shifted maximum and slope in its ξ dependence:

$$w(y,k,b) = 0.358\,\exp\Big(-0.402(\xi-0.756)^2\Big). \tag{28}$$

Of course the shift in the maximum corresponds to a universal enhancement of the value of the saturation momentum.

Numerical calculations of the single inclusive cross-section along these formulas were performed in [17]. However such calculations for the double inclusive cross-sections look very difficult, so that we shall instead use analytical estimates obtained in the asymptotic regime when both $Y-y$ and y are large. Then we can use the well known asymptotic expressions

for the BFKL Green function to obtain an explicit expression for function $h^{(0)}$. Repeating the calculations done in [14] we obtain

$$J_1(y,k,b) = \frac{8\bar{\alpha}}{k^2} R_P e^{\Delta(Y-y)} \sqrt{\frac{\pi}{\beta(Y-y)}} F(y,k,b), \tag{29}$$

where $\Delta = 4\ln 2\bar{\alpha}$ is the BFKL intercept, $\beta = 14\zeta(3)\bar{\alpha}$, R_P is the radius of the projectile and

$$F(y,k,b) = \int \frac{d^2q}{2\pi q} w(y,k-q,b) = Q_s(y,b) f(\hat{k}), \quad \hat{k} = \frac{k}{Q_s(y,b)}. \tag{30}$$

Function $f(\hat{k})$ obviously reduces to a constant $f(0)$ when $k \ll Q_s$. In the opposite case when $k \gg Q_s$ it behaves as $\lambda/\hat{k}$. Numerical calculations give values for $f(k)$ illustrated in Fig. 3 with

$$f(0) = 3.97, \quad \lambda = 54.6\,. \tag{31}$$

So for momenta considerably below the saturation momentum we find

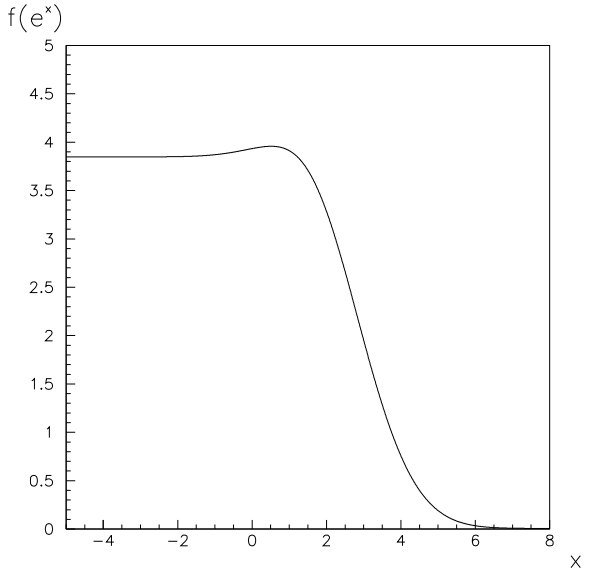

Figure 3: Function $f(e^x)$.

$$J_1(y,k,b) = \frac{8\bar{\alpha}}{k^2} R_P f(0) e^{\Delta(Y-y)} \sqrt{\frac{\pi}{\beta(Y-y)}} Q_s(y,b) \tag{32}$$

and for momenta considerably above the saturation momentum

$$J_1(y,k,b) = \frac{8\bar{\alpha}}{k^3} R_P \lambda e^{\Delta(Y-y)} \sqrt{\frac{\pi}{\beta(Y-y)}} Q^2(y,b)\,. \tag{33}$$

The found cross-section grows exponentially with the overall rapidity Y, which just reflects the growth of the pomeron directly coupled to the projectile. One expects that for an extended projectile this growth would be finally tempered when more than one pomeron are coupled

to it (see Fig. 4), contributions which are damped by powers of the small coupling constant for a point-like projectile. As we shall see, in the expression for the correlation coefficient the growing factors cancel, so that the resulting coefficient depends on Y only weakly. For this reason we may hope that our formulas remain applicable also for realistic hadrons. Another

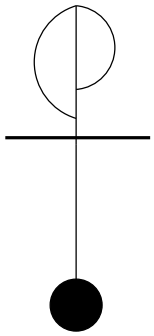

Figure 4: Diagrams not taken into account for the total cross-section for a point-like projectile.

interesting feature is the peculiar dependence on the nuclear factor $\Big(AT(b)\Big)^p$, with $p = 2/3$ for $k \ll Q_s$ and $p = 4/3$ for $k \gg Q_s$, which is of primary importance for the correlations. Integration over b and division by Σ leads to multiplicities in these two regions of k. For $k \ll Q_s$

$$M_1(y,k) = A^{2/9}\frac{3}{8}\gamma\frac{8\bar{\alpha}}{k^2}R_P f(0)e^{\Delta Y-\epsilon y}\sqrt{\frac{\pi}{\beta y(Y-y)}}, \tag{34}$$

where

$$\gamma = a\Big(\frac{9}{4\pi^2}\Big)^{1/3} \tag{35}$$

and $\epsilon = \Delta - \Delta_1$, and for $k \gg Q_s$

$$M_1(y,k) = A^{4/9}\frac{3}{10}\gamma^2\frac{8\bar{\alpha}}{k^3}R_P\lambda e^{\Delta Y-\epsilon_1 y}\sqrt{\frac{\pi}{\beta y^2(Y-y)}}, \tag{36}$$

with $\epsilon_1 = \Delta - 2\Delta_1$.

3.3 Double inclusive cross-section and correlations

The double inclusive cross-section is described by a set of diagrams shown in Fig. 5 (a few evident additional diagrams are not shown). They are quite complicated, especially since the cut vertex appearing in the diagram Fig. 5 f is different from the uncut one [18]. As mentioned in the Introduction, a detailed calculation of all the contributions does not seem very realistic. However at high values of all rapidity distances, $Y - y_1, Y - y_2, y_1, y_2 \gg 1$, of all the contributions the dominant ones correspond to Figs. 5 c-e, in which the upper vertex can have rapidities up to Y, so that the two pomeron lines below give the maximally growing exponential factor $\exp\Big(\Delta(2Y - y_1 - y_2)\Big)$. The relative weights of all other contributions is

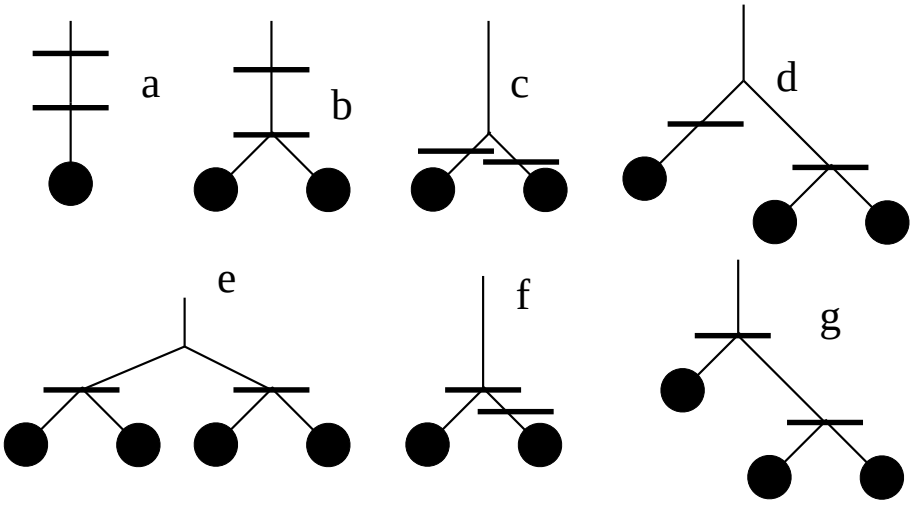

Figure 5: Diagrams contributing to the double inclusive cross-section in perturbative QCD.

exponentially damped. The study of contributions from all the diagrams of Fig. 5 *c*-*e* can be done by the same method which was used in [14] for the diagram of Fig. 5 *c*. Contribution of the diagrams 5. *d* and *e* can be taken into account by changing function $h(y,q,r)$ to $w(y,q,h)$ in all the formulas. In this way we obtain the double inclusive cross-section as

$$J_2(y_1,k_1;y_2,k_2,b) =$$
$$\frac{4}{\ln 2}\frac{\bar{\alpha}^2}{k_1^2k_2^2}\langle r^2\rangle_P e^{\Delta(2Y-y_1-y_2)}\sqrt{\frac{\pi}{\beta(2Y-y_1-y_2)}}F(y_1,k_1,b)F(y_2,k_2,b), \tag{37}$$

where F is the same function (30). Further simplifications, similarly to the case of single inclusive cross-sections, can be made when k_1 and k_2 are either much smaller than the saturation momentum or much larger than it. In the case when both $k_1 \ll Q_s$ and $k_2 \ll Q_s$

$$J_2 = \frac{4}{\ln 2}\frac{\bar{\alpha}^2}{k_1^2k_2^2}\langle r^2\rangle_P f^2(0) e^{\Delta(2Y-y_1-y_2)}\sqrt{\frac{\pi}{\beta(2Y-y_1-y_2)}}Q_s(y_1,b)Q_s(y_2,b). \tag{38}$$

If both $k_1 \gg Q_s$ and $k_2 \gg Q_s$ then

$$J_2 = \frac{4}{\ln 2}\frac{\bar{\alpha}^2}{k_1^3k_2^3}\langle r^2\rangle_P \lambda^2 e^{\Delta(2Y-y_1-y_2)}\sqrt{\frac{\pi}{\beta(2Y-y_1-y_2)}}Q_s^2(y_1,b)Q_s^2(y_2,b). \tag{39}$$

Finally in the case $k_1 \gg Q_s$ and $k_2 \ll Q_s$ we find

$$J_2 = \frac{4}{\ln 2}\frac{\bar{\alpha}^2}{k_1^3k_2^2}\langle r^2\rangle_P \lambda f(0) e^{\Delta(2Y-y_1-y_2)}\sqrt{\frac{\pi}{\beta(2Y-y_1-y_2)}}Q_s^2(y_1,b)Q_s(y_2,b). \tag{40}$$

Integration over b and division by Σ leads to the corresponding multiplicities $M_2(y_1,k_1;y_2,k_2)$. In the case when both $k_1 \ll Q_s$ and $k_2 \ll Q_s$

$$M_2 = A^{4/9}\frac{3}{10}\gamma^2\frac{4}{\ln 2}\frac{\bar{\alpha}^2}{k_1^2k_2^2}\langle r^2\rangle_P f^2(0) e^{2\Delta Y-\epsilon(y_1+y_2)}\sqrt{\frac{\pi}{\beta y_1y_2(2Y-y_1-y_2)}}. \tag{41}$$

If both $k_1 \gg Q_s$ and $k_2 \gg Q_s$ then

$$M_2 = A^{8/9}\frac{3}{14}\frac{4}{\ln 2}\frac{\bar{\alpha}^2}{k_1^3 k_2^3}\langle r^2\rangle_P \lambda^2\gamma^4 e^{2\Delta Y-\epsilon_1(y_1+y_2)}\sqrt{\frac{\pi}{\beta y_1^2 y_2^2(2Y-y_1-y_2)}}. \tag{42}$$

Finally in the case $k_1 \gg Q_s$ and $k_2 \ll Q_s$ we find

$$M_2 = A^{2/3}\frac{1}{4}\frac{4}{\ln 2}\frac{\bar{\alpha}^2}{k_1^3 k_2^2}\langle r^2\rangle_P \lambda f(0)\gamma^3 e^{2\Delta Y-\epsilon_1 y_1-\epsilon y_2}\sqrt{\frac{\pi}{\beta y_1^2 y_2(2Y-y_1-y_2)}}. \tag{43}$$

It is convenient to introduce a ratio

$$R(y_1,k_1;y_2,k_2) = \frac{M_2(y_1,k_1;y_2,k_2)}{M_1(y_1,k_1)M_1(y_2,k_2)}, \tag{44}$$

for which for all three limiting cases considered above we obtain a simple expression:

$$R(y_1,k_1;y_2,k_2) = C\frac{1}{16\ln 2}\frac{\langle r^2\rangle_P}{R_P^2}\sqrt{\frac{\beta(Y-y_1)(Y-y_2)}{\pi(2Y-y_1-y_2)}}, \tag{45}$$

where for the cases $k_1,k_2 \ll Q_s$, $k_1,k_2 \gg Q_s$ and $k_1 \gg Q_s, k_2 \ll Q_s$ the coefficient C is 32/15, 50/21 and 20/9 respectively. If the two produced jets of hadrons are taken symmetric in the c.m. system for hN collisions with the rapidity distance y then

$$y_1 = \frac{1}{2}(Y+y), \quad y_2 = \frac{1}{2}(Y-y), \tag{46}$$

and

$$R(y_1,k_1;y_2,k_2) = C\frac{1}{32\ln 2}\frac{\langle r^2\rangle_P}{R_P^2}\sqrt{\frac{\beta}{\pi}}\,\Gamma(y_1,y_2), \tag{47}$$

with

$$\Gamma(y_1,y_2) = \sqrt{Y-\frac{y^2}{Y}}, \quad \Gamma(y_1,y_1) = \sqrt{Y-y}, \quad \Gamma(y_2,y_2) = \sqrt{Y+y}. \tag{48}$$

Eqs. (45), (47) and (48) are the central result of this Section.

In terms of the ratio R the correlation coefficient is given by

$$B = \frac{M_1(y_B,k_B)}{M_1(y_F,k_F)}\frac{R(y_F,k_F;y_B,k_B)-1}{R(y_F,k_F;y_F,k_F)-1}. \tag{49}$$

The coefficient in Eq. (47) is very small e.g. ~ 0.1 for $\alpha_s \simeq 0.2$. Thus both the numerator and denominator in this equation are negative except for very large energies ($Y > 100$ in the mentioned example). Furthermore, R may be smaller than one for some small window in y and Y, but it is generically larger than one. To illustrate it, at large Y and fixed y we conclude from (47) that R is independent of y in all cases. So if k_F and k_B have the same order of magnitude (either much smaller or much larger than Q_s) the second ratio in (49) is equal to unity. In this case we have a simple result

$$B = \frac{M_1(y_B,k_B)}{M_1(y_F,k_F)}\,. \tag{50}$$

For the most important case from the practical point of view, $k_F, k_B \ll Q_s$, we then find

$$B = \frac{k_F^2}{k_B^2} e^{\epsilon y}, \tag{51}$$

or for windows symmetric also in the phase volume of transverse momenta simply

$$B = e^{\epsilon y}\,. \tag{52}$$

The concrete value of ϵ depends on the chosen value for α_s. With a typical value $\alpha_s = 0.2$ we find $\epsilon \simeq 0.1 \div 0.15$.

It is not difficult to obtain predictions for B for all other theoretically possible cases. If both k_F and k_B are much larger than the saturation momentum we obtain the correlation coefficient (52) with ϵ substituted by ϵ_1. In still more exotic cases, when one of the momenta is much smaller and the other much larger than Q_s, the second ratio in (49) begins to depend on Y non-trivially because of different coefficients C in (47). Also a nontrivial dependence on A appears, due to different powers of A in (34) and (36). The explicit formulas can be easily written using (34), (36) and (47). We do not present them due to a small probability of the corresponding experimental setup.

As we see in all cases the correlation coefficient turns out to be different from the probabilistic predictions. For symmetric windows it is independent of A, generically greater than unity and grows (rather slowly) with the rapidity distance.

4 Color Glass Condensate

In this Section we follow the lines in [5, 6] to obtain an expression for the correlation strength B in hadron-nucleus, pA collisions, considering the hadron as a saturated object with some saturation scale $Q_{s,p}^2(y) < Q_{s,A}^2(y) \propto A^\delta$, $\delta > 0$, as done in [19, 20]. For the multiplicity of produced gluons, one gets in a small overlap area a^2 (with $a \ll R_0$ corresponding to the correlation length of the classical fields) between projectile and target:

$$\left\langle \frac{dN}{dy} \right\rangle \sim \frac{Q_{s,min}^2(y)}{\alpha_s\left(Q_{s,min}(y)\right)}\, a^2, \quad Q_{s,min}^2(y) = \min\left\{Q_{s,p}^2(y), Q_{s,A}^2(y)\right\}. \tag{53}$$

After integration over impact parameter one gets an overlap area S i.e.

$$\left\langle \frac{dN}{dy} \right\rangle \sim \frac{Q_{s,min}^2(y)}{\alpha_s\left(Q_{s,min}(y)\right)}\, S \tag{54}$$

such that $SQ_{s,h}^2 \propto N_{part,h}$, the number of nucleons from hadron h participating in the collision ($N_{part,p} \equiv 1$), see also [20].

The numerator in Eq. (8) (coming from diagrams like that in Fig. 6 *a*) results in

$$\left\langle \frac{dN}{dy_F}\frac{dN}{dy_B} \right\rangle - \left\langle \frac{dN}{dy_F} \right\rangle \left\langle \frac{dN}{dy_B} \right\rangle \sim \frac{Q_{s,min}^2(y_F)}{\alpha_s\left(Q_{s,min}(y_F)\right)} \frac{Q_{s,min}^2(y_B)}{\alpha_s\left(Q_{s,min}(y_B)\right)}\, a^4. \tag{55}$$

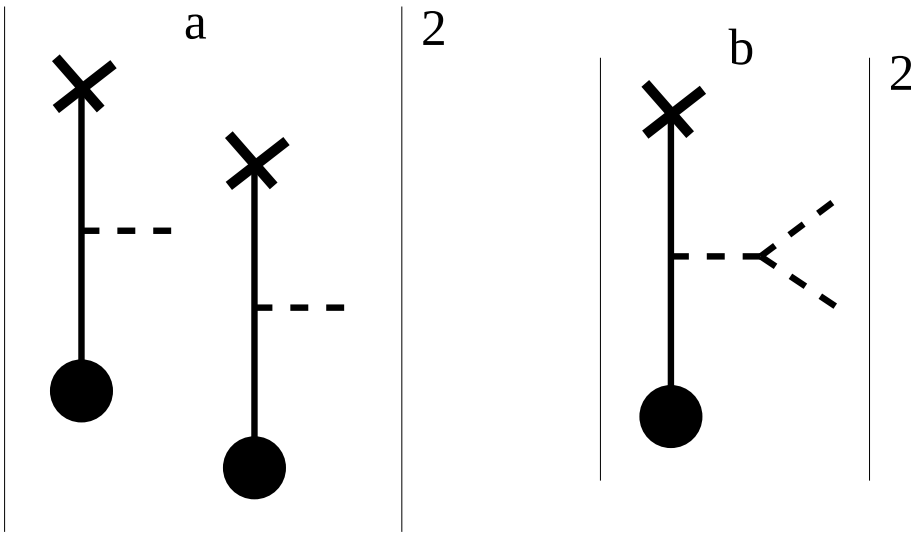

Figure 6: Diagrams contributing to the double inclusive cross-section in the CGC. The black dot and the cross correspond to the projectile and the target from which the classical fields, represented by the solid lines, come. The dashed lines represent the emitted gluons.

Now, for the integration over impact parameter we consider that $a^2 \sim 1/Q^2_{s,max}(y_F, y_B)$, $Q^2_{s,max}(y_F, y_B) = \max\left\{Q^2_{s,p}(y_F), Q^2_{s,A}(y_F), Q^2_{s,p}(y_B), Q^2_{s,A}(y_B)\right\}$, which results in

$$\left\langle \frac{dN}{dy_F}\frac{dN}{dy_B}\right\rangle - \left\langle \frac{dN}{dy_F}\right\rangle\left\langle \frac{dN}{dy_B}\right\rangle \sim \frac{Q^2_{s,min}(y_F)}{\alpha_s\left(Q_{s,min}(y_F)\right)}\frac{Q^2_{s,min}(y_B)}{\alpha_s\left(Q_{s,min}(y_B)\right)}\frac{S}{Q^2_{s,max}(y_F, y_B)}. \quad (56)$$

For the denominator in Eq. (8) there is an additional piece coming from diagrams like that in Fig. 6 *b*,

$$\left[\left\langle \frac{dN}{dy_F}\frac{dN}{dy_B}\right\rangle - \left\langle \frac{dN}{dy_F}\right\rangle\left\langle \frac{dN}{dy_B}\right\rangle\right]' \sim Q_{s,min}(y_F)Q_{s,min}(y_B)e^{-\kappa(y_F-y_B)}S. \quad (57)$$

As discussed in [6], this piece is $\mathcal{O}(\alpha_s^2)$ suppressed compared to (56). It contains an exponential damping factor, with $\kappa \sim 1$, which motivates its absence in the numerator for large enough $y_F - y_B$.

Neglecting any possible interference between these two kinds of diagrams, the final expression for Eq. (8) reads

$$B = \left[1 + c\,\frac{\alpha_s\left(Q_{s,min}(y_F)\right)\alpha_s\left(Q_{s,min}(y_B)\right)}{Q_{s,min}(y_F)Q_{s,min}(y_B)}\,Q^2_{s,max}(y_F, y_B)\right]^{-1}, \quad (58)$$

where c is a constant. Note that for AA collisions and symmetric intervals $y_B = -y_F$, this expression reduces to that found in [6], $B = \left[1 + c\alpha_s^2\right]^{-1}$, from which the correlation strength was argued to increase with centrality and energy of the collision. For the asymmetric case Eq. (58), the latter behavior is the same, while the dependence on centrality or nuclear size depends on the rapidities y_F, y_B.

To illustrate this latter behavior, let us take the parametrizations [20]

$$Q_{s,p}^2(y) = Q_0^2 \left(\frac{Q_0}{E_{cm}}\right)^{\lambda} e^{-\lambda y}, \quad Q_{s,A}^2(y) = Q_{s,p}^2\left(-y, Q_0^2 \to Q_0^2 A^{1/3}\right), \tag{59}$$

with Q_0^2 a constant with dimension of momentum squared, E_{cm} the collision energy in the center-of-mass system, $\lambda \sim 0.3$, and rapidities defined in the center-of-mass system in which the projectile is located at $y = Y/2$ and the nuclear target at $y = -Y/2$. The solution of the equation

$$Q_{s,p}^2(y_c) = Q_{s,A}^2(y_c) \tag{60}$$

defines [20] a critical rapidity $y_c \simeq -4 \div -3 < 0$ such that for $y < y_c$, $Q_{s,min}^2(y) = Q_{s,A}^2(y)$, while for $y > y_c$, $Q_{s,min}^2(y) = Q_{s,p}^2(y)$. Let us examine several situations:

- For $y_c < y_B = -y_F$ - the most feasible situation from the experimental point of view, $Q_{s,min}(y_F) = Q_{s,p}(y_F)$, $Q_{s,min}(y_B) = Q_{s,p}(y_B)$ and $Q_{s,max}(y_F, y_B) = Q_{s,A}(y_F)$, the correlation strength B decreases with increasing A.

- For $y_B = -y_F < y_c$, $Q_{s,min}(y_F) = Q_{s,p}(y_F)$, $Q_{s,min}(y_B) = Q_{s,A}(y_B)$ and $Q_{s,max}(y_F, y_B) = Q_{s,A}(y_F)$. Provided the power-law behavior in (59) dominates over the logarithmic behavior of the running coupling, the correlation strength B also decreases with increasing A but more slowly than in the previous case.

- For $y_B < y_F < y_c$ (a situation within the kinematical reach of the Large Hadron Collider (LHC) with e.g. $y_B = -7$ and $y_F = -5$), $Q_{s,min}(y_F) = Q_{s,A}(y_F)$, $Q_{s,min}(y_B) = Q_{s,A}(y_B)$ and $Q_{s,max}(y_F, y_B) = Q_{s,p}(y_B)$, the correlation strength B increases with increasing A.

The results in this Section should be applicable for transverse momenta of the order or smaller that the corresponding saturation scales. In any case, the correlation strength is always smaller than 1, a behavior opposite to that generically found in the previous Section, see e.g. (52). The difference is most probably due to the fact that in that Section, the hadron was always considered a dilute object i.e. no saturation scale was assigned to it, the coupling to the projectile being always given by a single pomeron, and to the asymptotic limits taken there.

5 Conclusions

In this paper we analyze the long-range rapidity correlations in hadron-nucleus collisions. First we recall the standard results in the probabilistic model. The correlation strength B

shows an increasing behavior with increasing nuclear size or centrality, tending to unity for $A \to \infty$.

Next we turn to perturbative QCD. We consider interacting BFKL pomerons in the form of fan diagrams coupled to a dilute projectile. After examining the required single and double inclusive cross-sections [17, 18], analytic estimates are done for very large rapidities due to the difficulties for a complete consideration of the double inclusive density. The correlation strength results weakly depending on energy and centrality or nuclear size, and generically greater than unity. Note that these results are rigorously applicable to DIS, but require certain caution if applied to hA scattering with ordinary hadrons.

Finally, we turn to the Color Glass Condensate framework. Taking the projectile as a saturated object characterized by a saturation scale smaller - as expected - than that of the nucleus, we extend to asymmetric collisions the analysis done in [5, 6] for nucleus-nucleus collisions. The resulting correlation strength turns out to be smaller than unity and increasing with increasing energy. Its behavior with increasing centrality or nuclear size depends on the considered rapidity windows but generically decreases for the most feasible experimental situation.

A note of caution is in order. The correlations considered in this paper are those coming from particle production in the initial stage of the collision. Subsequent stages may modify the predicted behaviors. In any case, hadron-nucleus collisions should offer a more reliable setup than nucleus-nucleus in this respect, as the production of a dense, eventually thermalized medium is not expected. Besides, hadronic rescattering of the produced secondaries is expected to play a little role except in the region close to the rapidity of the nucleus. With all these caveats in mind, phenomenological applications of our results to dAu collisions at the Relativistic Heavy Ion Collider and pA collisions at the LHC are the obvious extension of this work.

6 Acknowledgments

MAB has been financially supported by grants RNP 2.1.1.1112 and RFFI 06-02-16115a of Russia, and NA and CP by Ministerio de Educación y Ciencia of Spain under project FPA2005-01963 and by Xunta de Galicia (Consellería de Educación). NA also acknowledges financial support by Ministerio de Educación y Ciencia of Spain under a contract Ramón y Cajal. We thank J.Dias de Deus, F.Gelis, L.McLerran, A.H.Mueller and B.Srivastava for useful discussions. MAB also thanks Departamento de Física de Partículas of the Universidade de Santiago de Compostela for warm hospitality.

References

[1] A.Capella and J.Tran Than Van, Phys. Rev. **D 29** (1984) 2512.

[2] N.Armesto, M.A.Braun, E.G.Ferreiro and C.Pajares, Phys. Rev. Lett. **77** (1996) 3736.

[3] N.S.Amelin, N.Armesto, M.A.Braun, E.G.Ferreiro and C.Pajares, Phys. Rev. Lett. **73** (1994) 2813.

[4] M.A.Braun, R.S.Kolevatov, C.Pajares and V.V.Vechernin, Eur. Phys. J. **C32** (2004) 535.

[5] Yu.V.Kovchegov, E.Levin and L.McLerran, Phys. Rev. **C 63** (2001) 024903.

[6] N.Armesto, L.McLerran and C.Pajares, Nucl. Phys. **A 781** (2007) 201.

[7] L.McLerran and R.Venugopalan, Phys. Rev. **D 49** (1994) 2233, 3352; **D 50** (1994) 2225.

[8] I.I.Balitsky, Nucl. Phys. **B463** (1996) 99.

[9] Yu.V.Kovchegov, Phys. Rev. **D60** (1999) 034008; **D61** (2000) 074018.

[10] M.A.Braun, Eur. Phys. J **C16** (2000) 337.

[11] L.N.Lipatov in "Perturbative QCD", Ed. A.H.Mueller, World Scientific, Singapore (1989), p. 411.

[12] N.Armesto and M.A.Braun, Eur. Phys. J. **C20** (2001) 517; **C22** (2001) 351.

[13] J.L.Albacete, N.Armesto, J.G.Milhano, C.A.Salgado and U.A.Wiedemann, Phys. Rev. **D71** (2005) 014003.

[14] M.A.Braun, Phys. Lett. **B483** (2000) 105.

[15] Yu.V.Kovchegov and K.Tuchin, Phys. Rev. **D65** (2002) 074026.

[16] V.A.Abramovsky, V.N.Gribov and O.V.Kancheli, Sov. J. Nucl. Phys. **18** (1974) 308.

[17] M.A.Braun, Eur. Phys. J. **C39** (2005) 451.

[18] M.A.Braun, Eur. Phys. J. **C48** (2006) 501.

[19] A.Dumitru and L.D.McLerran, Nucl. Phys. **A700** (2002) 492.

[20] D.Kharzeev, E.Levin and M.Nardi, Nucl. Phys. **A730** (2004) 448 [Erratum-ibid. **A743** (2004) 329].